The New Low-Band Gap Polymers Comprising C-, Si-, or N-Bridged Dithiophene and Alkoxy-Modified 2,1,3-Benzooxadiazole Units for Bulk Heterojunction Solar Cells

Jian-Ming Jiang, Po-An Yang, Chia-Ming Yu, His-Kuei Lin, Kuei-Chun Huang, Kung-Hwa Wei

Department of Materials Science and Engineering, National Chiao Tung University, Hsinchu 300, Taiwan
Correspondence to: K.-H. Wei (E-mail: khwei@mail.nctu.edu.tw)

Received 21 April 2012; accepted 2 June 2012; published online 5 July 2012
DOI: 10.1002/pola.26216

ABSTRACT: In this study, we used Stille coupling polymerization to synthesize a series of new low-band gap-conjugated polymers—**PCyTBO**, **PCySiTBO**, and **PCyNTBO**—comprising mainly electron-rich C-, Si-, and N-bridged dithiophene units in conjugation with electron-deficient alkoxy-modified 2,1,3-benzooxadiazole moieties. The highest occupied molecular orbital energy levels of these polymers become higher as the electron-donating ability of C-, Si-, or N-bridged dithiophene units increases. These polymers also displayed excellent thermal stability and broad spectral absorptions, with **PCySiTBO** revealing some crystallinity. As a result, the photovoltaic device incorporating the **PCySiTBO**/$PC_{71}BM$ (1:1) blend system and 1,8-diiodooctane (2 vol %) as an additive exhibited excellent performance, under AM 1.5 G irradiation (100 mW cm^{-2}), with a value of V_{oc} of 0.64 V, a short-circuit current density of 13.8 mA cm^{-2}, a fill factor of 0.57, and a promising power conversion efficiency of 5.0%. © 2012 Wiley Periodicals, Inc. J Polym Sci Part A: Polym Chem 50: 3960–3969, 2012

KEYWORDS: benzooxadiazole; donor/acceptor conjugated polymers; polymer solar cell

INTRODUCTION Organic polymer solar cells (PSCs) based on bulk heterojunction (BHJ) structures incorporating conjugated polymers and fullerenes are being studied extensively because they allow the fabrication of light-weight, large-area, flexible devices using low-cost solution processing methods.[1–3] Poly[2-methoxy-5-(3′,7′-dimethyloctyloxy)-1,4-phenylene vinylene] (MDMO-PPV),[4] because of its relatively low highest-occupied molecular orbital (HOMO) energy level of −5.4 eV, BHJ devices made from MDMO-PPV offered open circuit voltages (V_{oc}) as high as 0.82 V; however, the relatively large band gap of MDMO-PPV limited the short circuit current density (J_{sc}) to 5–6 mA/cm^2. As a result, conjugated polymers such as regioregular polythiophene derivatives have been employed widely in BHJ devices because of their high crystallinity, good light harvesting in the visible spectrum, and excellent carrier mobility.[5–7] Nevertheless, the power conversion efficiencies (PCEs) of such systems are difficult to improve upon because of the limited polymer absorption at wavelengths of $<$650 nm[8] and because the V_{oc} is limited at approximately 0.5–0.6 V.

In attempts to harvest more photons and to tune the energy levels, several conjugated polymers have been developed featuring electron donor/acceptor (D/A) units in main chain-conjugated configurations[9–19] and side-chain-attached architectures.[20–24] Recently, some low-band gap polymers have been developed to provide PCEs of up to 7%.[25–29] To improve the performance of photovoltaic polymer materials, it will be necessary to synthesize conjugated polymers with several desirable properties: low-band gaps, to broaden the absorption range; crystalline characteristics, to ensure good charge mobility; low HOMO energy levels, to enhance the values of V_{oc}; and lowest unoccupied molecular orbital (LUMO) energy levels that are suitable for efficient electron transfer to the fullerene moieties.

During the last few years, 4*H*-cyclopenta[2,1-*b*:3,4-*b*′]-dithiophene (Cy) has emerged as an attractive building block for organic photovoltaics; it exhibits good electron-donating properties, features a rigid coplanar structure favoring intermolecular π–π interactions, and allows straightforward side-chain manipulation to influence solubility and processability.[30–32] By changing the bridging atom from C to Si, silole-containing polymers with low-lying HOMO energy levels have been developed to enhance the V_{oc}.[33–35] In addition, silole-containing polymers applied in photovoltaic devices have also proved to be effective at improving hole mobility and rendering higher crystallinity. Compared with the C- and Si-bridged dithiophenes, dithieno[3,2-*b*:2′,3′-*d*]pyrrole (CyN), the corresponding N-bridged dithiophene, possesses stronger electron-donating ability, and has been used as an electron-rich donor for D/A-conjugated polymers exhibiting broad

absorption (reaching 1000 nm). BHJ cells derived from these polymers have, however, provided PCEs of 2.1 and 2.7%,[36,37] owing to the low values of V_{oc} of these devices. Therefore, to improve device performance, we must develop polymers with optimal LUMO and HOMO energy levels and charge transporting properties.

Recently, devices based on polymers containing benzooxadiazole (BO) units and several thiophene-based building blocks exhibiting high values of V_{oc}[38] have been reported. Those studies inspired us to further explore the possibility of using alkoxy-modified BO copolymerized with electron-rich bridged dithiophenes to improve the applicability of the polymer. In this article, considering not only the electron energy levels but also the hole mobilities, we present a series of new D/A alternating polymers based on C-, Si-, and N-bridged dithiophenes as electron-rich donors and alkoxy-modified BO units as electron-deficient acceptors—**PCyTBO**, **PCySiTBO**, and **PCyNTBO**—wherein the electron-withdrawing BO units were conjugated with the electron-donating units to provide crystalline characteristics and low-band gap polymers. Because of these desirable features, we expected **PCyTBO**, **PCySiTBO**, and **PCyNTBO** to exhibit good hole mobilities and broad absorption wavelengths suitable for photovoltaic applications.

EXPERIMENTAL

Materials and Synthesis

4,7-*Bis*(5-bromothien-2-yl)-5,6-*bis*(octyloxy)benzo[c][1,2,5]oxadiazole (**M1**)[12] (4,4-Dioctyl-4*H*-cyclopenta[1,2-*b*:5,4-*b*′]dithiophene-2,6-diyl)*bis*(trimethylstannane) (**M2**),[30] 4,4-dioctyl-2,6-*bis*(trimethylstannyl)-4*H*-silolo[3,2-*b*:4,5-*b*′]dithiophene (**M3**),[35] and 4-(heptadecan-9-yl)-2,6-*bis*(trimethylstannyl)-4*H*-dithieno[3,2-*b*:2′,3′-*d*]pyrrole (**M4**)[39] were prepared according to the reported procedures. [6,6]-Phenyl-C_{61}-butyric acid methyl ester ($PC_{61}BM$) and [6,6]-Phenyl-C_{71}-butyric acid methyl ester ($PC_{71}BM$) were purchased from Nano-C. All other reagents were used as received without further purification, unless stated otherwise.

General Procedure for Stille Polymerization: Alternating Polymer PCyTBO

M1 (100 mg, 0.143 mmol), **M2** (104.3 mg, 0.143 mmol), and tri-*o*-tolylphosphine (3.5 mg, 8.0 mol %) were dissolved in dry chlorobenzene (CB; 4 mL) and degassed for 15 min. Pd_2dba_3 (2.6 mg, 2.0 mol %) was added under N_2 and then the reaction mixture was heated at 130°C for 48 h. After cooling to room temperature, the solution was added dropwise into MeOH (100 mL). The crude polymer was collected, dissolved in $CHCl_3$, and reprecipitated from MeOH. The solid was washed with MeOH, acetone, and $CHCl_3$ in a Soxhlet apparatus. The $CHCl_3$ solution was concentrated and then added dropwise into MeOH. The precipitate was collected and dried under vacuum to give **PCyTBO** (97 mg, 70%). ^{1}H NMR (300 MHz, $CDCl_3$): δ 8.03–7.88 (m, 2H), 7.58–7.03 (m, 4H), 4.02 (br, 4H), 2.07 (br, 4H), 1.58–0.96 (m, 48H), 0.79 (s, 12H). Anal. Calcd: C, 70.61; H, 8.32; N, 2.89. Found: C, 71.23; H, 8.91; N, 3.15.

Alternating Polymer PCySiTBO

Using a polymerization procedure similar to that described above for **PCyTBO**, a mixture of **M1** (100 mg, 0.143 mmol) and **M3** (106.6 mg, 0.143 mmol) in dry CB (4 mL) was polymerized to give **PCySiTBO** (105 mg, 75%). ^{1}H NMR (300 MHz, $CDCl_3$): δ 8.15–7.92 (m, 2H), 7.58–6.98 (m, 4H), 4.02 (br, 4H), 2.08 (br, 4H), 1.58–0.96 (m, 48H), 0.83 (s, 12H). Anal. Calcd: C, 68.24; H, 8.18; N, 2.84. Found: C, 68.75; H, 8.37; N, 2.36.

Alternating Polymer PCyNTBO

Using a polymerization procedure similar to that described above for **PCyTBO**, a mixture of **M1** (100 mg, 0.143 mmol) and **M4** (106.4 mg, 0.143 mmol) in dry CB (4 mL) was polymerized to give **PCyNTBO** (90 mg, 65%). ^{1}H NMR (300 MHz, $CDCl_3$): δ 8.03–7.72 (m, 2H), 7.59–7.03 (m, 4H), 4.05 (br, 4H), 3.62 (br, 1H), 2.07 (br, 4H), 1.62–0.98 (m, 48H), 0.81 (s, 12H). Anal. Calcd: C, 69.54; H, 8.29; N, 4.27. Found: C, 70.15; H, 8.02; N, 4.56.

Measurements and Characterization

^{1}H NMR spectra were recorded using a Varian UNITY 300-MHz spectrometer. Thermogravimetric analysis (TGA) was performed using a TA Instruments Q500 apparatus; the thermal stabilities of the samples were determined under a N_2 atmosphere by measuring their weight losses while heating at a rate of 20°C min^{-1}. Size exclusion chromatography (SEC) was performed using a Waters chromatography unit interfaced with a Waters 1515 differential refractometer; polystyrene was the standard; the temperature of the system was set at 45°C; tetrahydrofuran (THF) was the eluent. UV–Vis spectra of dilute samples in dichlorobenzene (DCB) solutions (1×10^{-5} M) were recorded at room temperature (ca. 25°C) using a Hitachi U-4100 spectrophotometer. Solid films for UV–Vis spectroscopic analysis were obtained by spin-coating the polymer solutions onto a quartz substrate. Cyclic voltammetry (CV) of the polymer films was performed using a BAS 100 electrochemical analyzer operated at a scan rate of 50 mV s^{-1}; the solvent was anhydrous MeCN, containing 0.1 M tetrabutylammonium hexafluorophosphate ($TBAPF_6$) as the supporting electrolyte. The potentials were measured against an Ag/Ag^+ (0.01 M $AgNO_3$) reference electrode; the ferrocene/ferrocenium ion (Fc/Fc^+) pair was used as the internal standard (0.09 V). The onset potentials were determined from the intersection of two tangents drawn at the rising and background currents of the cyclic voltammograms. HOMO and LUMO energy levels were estimated relative to the energy level of the ferrocene reference (4.8 eV below vacuum level). X-ray diffraction patterns of the pristine polymer thin films were measured using a Bruker D8 high-resolution X-ray diffractometer operated in grazing incidence mode. Topographic and phase images of the polymer:PCBM films (surface area: 5×5 μm^2) were obtained using a Digital Nanoscope III atomic force microscope (AFM) operated in the tapping mode under ambient conditions. The thickness of the active layer of the device was measured using a Veeco Dektak 150 surface profiler. Transmission electron microscopy (TEM) images of the polymer:PCBM films were

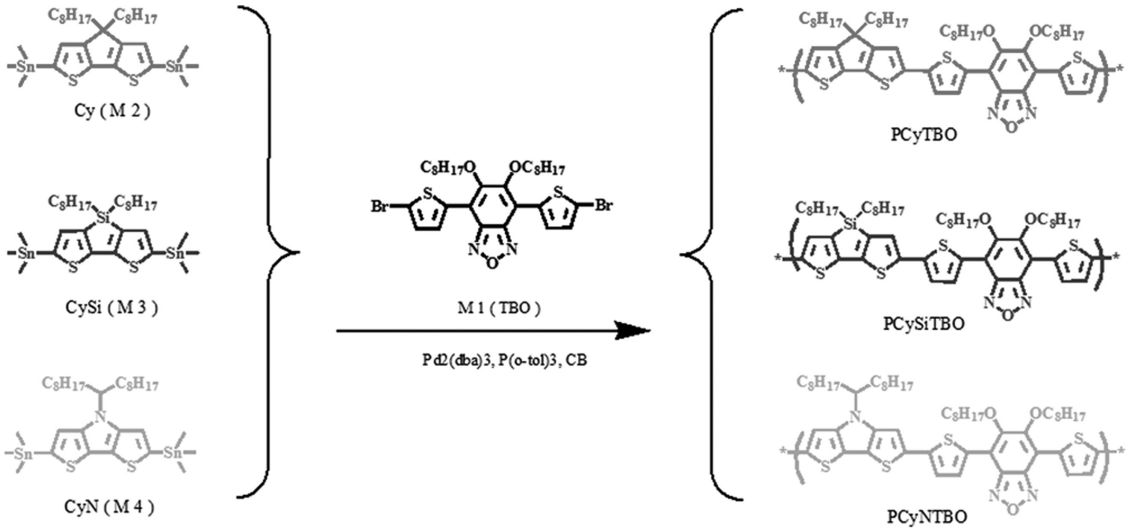

SCHEME 1 Synthesis and structures of the polymers **PCyTBO**, **PCySiTBO**, and **PCyNTBO**.

recorded using a FEI T12 transmission electron microscope operated at 120 keV.

Fabrication and Characterization of Photovoltaic Devices

Indium tin oxide (ITO)-coated glass substrates were cleaned stepwise in detergent, water, acetone, and isopropyl alcohol (ultrasonication; 20 min each), and then dried in an oven for 1 h; subsequently, the substrates were treated with UV ozone for 30 min prior to use. A thin layer (ca. 20 nm) of poly (ethylenedioxythiophene):polystyrenesulfonate (PEDOT:PSS, Baytron P VP AI 4083) was spin-coated (5000 rpm) onto the ITO substrates. After baking at 140°C for 20 min in air, the substrates were transferred to a N_2-filled glovebox. The polymer and PCBM were codissolved in DCB at various weight ratios, but with a fixed total concentration (40 mg mL^{-1}). The blend solutions were stirred continuously for 12 h at 80°C and then filtered through a PTFE filter (0.2 μm); the photoactive layers were obtained by spin-coating (600–2000 rpm, 60 s) the blend solutions onto the ITO/PEDOT:PSS surfaces and then heating for 20 min at 100°C. The thickness of each photoactive layer was approximately 85–105 nm. The devices were ready for measurement after thermal deposition (pressure: ca. 1×10^{-6} mbar) of a 20-nm-thick film of Ca and then a 100-nm-thick Al film as the cathode. The effective layer area of one cell was 0.04 cm^2. The current density–voltage (*J–V*) characteristics were measured using a Keithley 2400 source meter. The photocurrent was measured under simulated AM 1.5 G illumination at 100 mW cm^{-2} using a Xe lamp-based Newport 66902 150-W solar simulator. A calibrated Si photodiode with a KG-5 filter was employed to confirm the illumination intensity. External quantum efficiencies (EQEs) were measured using an SRF50 system (Optosolar, Germany). A calibrated mono-silicon diode exhibiting a response at 300–800 nm was used as a reference. For hole mobility measurements, hole-only devices were fabricated having the structure ITO/PEDOT:PSS/polymer/Au. The hole mobility was determined by fitting the dark *J–V* curve into the space-charge-limited current method,[20,40] based on the equation

$$J = \frac{9}{8}\varepsilon_0\varepsilon_r\mu_h\frac{V^2}{L^3}$$

where ε_0 is the permittivity of free space, ε_r is the dielectric constant of the polymer which is assumed to be around 3 for the conjugated polymers, μ_h is the hole mobility, V is the voltage drop across the device, and L is the thickness of active layer.

RESULTS AND DISCUSSION

Synthesis and Characterization of the Polymers

Scheme 1 outline our general synthetic strategy for obtaining the monomers and the polymers. To ensure good solubility of the BO derivative **M1**, we positioned two octyloxy chains on the BO ring as in the previous reports.[12,38] We synthesized **M2**, **M3**, and **M4** using previously reported methods.[30,35,39] After Stille couplings using Pd_2dba_3 as catalyst in CB at 130°C for 48 h, we obtained the polymers **PCyTBO**, **PCySiTBO**, and **PCyNTBO** in yields of 65–75%. We determined the weight–average molecular weights (M_w) of these polymers (Table 1) through SEC, against polystyrene standards, in THF as the eluent.

Thermal Stability

We used TGA to determine the thermal stability of the polymers (Fig. 1). In air, the 5% weight–loss temperatures (T_d) of **PCyTBO**, **PCySiTBO**, and **PCyNTBO** were 316, 312, and 316°C, respectively. Thus, they all exhibited good thermal stability against O_2—an important characteristic for device fabrication and application.

Optical Properties

We recorded the normalized optical UV–Vis absorption spectra of the polymers from their dilute DCB solutions at room temperature and as spin-coated films on quartz substrates.

TABLE 1 Molecular Weights, Thermal Properties, and Hole Mobilities of the Polymers

Polymer	M_w[a] (kDa)	M_n[a] (kDa)	PDI[a]	T_d[b] (°C)	Mobility ($cm^2\ V^{-1}\ s^{-1}$)
PCyTBO	36.5	22.8	1.6	316	3.2×10^{-4}
PCySiTBO	45.4	25.2	1.8	312	9.8×10^{-4}
PCyNTBO	45.2	23.8	1.9	316	1.8×10^{-4}

[a] Values of M_n, M_w, and PDI of the polymers were determined through GPC (polystyrene standards; THF).

[b] The 5% weight-loss temperatures in air.

Figure 2(a) shows the absorption spectra of **PCyTBO**, **PCySiTBO**, and **PCyNTBO** in DCB at room temperature; Table 2 summarizes the optical data, including the absorption peak wavelengths ($\lambda_{max,abs}$), absorption edge wavelengths ($\lambda_{edge,abs}$), and the optical band gap (E_g^{opt}). All of the absorption spectra recorded from dilute DCB solutions featured two absorption bands: one at 350–470 nm, which we assign to localized π–π^* transitions, and another, broader band from 490 to 750 nm in the long wavelength region, corresponding to intramolecular charge transfer (ICT) between the acceptor (BO) and donor (C-, Si-, or N-bridged dithiophene) units. The absorption spectra of the three polymers in the solid state were similar to their corresponding solution spectra, with slight red-shifts (ca. 5–40 nm) of their absorption maxima, indicating that some intermolecular interactions existed in the solid state. The absorption edges for **PCyTBO**, **PCySiTBO**, and **PCyNTBO** (Table 2) corresponded to optical band gaps (E_g^{opt}) of 1.59, 1.64, and 1.59 eV, respectively.

Electrochemical Properties

We used CV to examine the electrochemical properties of the C-, Si-, and N-bridged dithiophene/BO–based copolymers and, thereby, determine their HOMO and LUMO energy levels. Figure 3 shows the electrochemical properties of the polymers as solid films; Table 3 summarizes the relevant data. Partially reversible *n*-doping/dedoping (reduction/reoxidation) processes occurred for these polymers in the negative potential range—except for **PCyNTBO**, which underwent an irreversible reduction. In addition, reversible *p*-doping/dedoping (oxidation/re-reduction) processes occurred in the positive potential range for each of these polymers. The onset oxidation potentials (E_{onset}^{ox}, vs. Ag/Ag^+) for **PCyTBO**, **PCySiTBO**, and **PCyNTBO** were 0.18, 0.22, and 0.09 V, respectively. The onset reduction potentials (E_{onset}^{red}) for **PCyTBO**, **PCySiTBO**, and **PCyNTBO** were −1.76, −1.76, and −1.99 V, respectively. On the basis of these onset

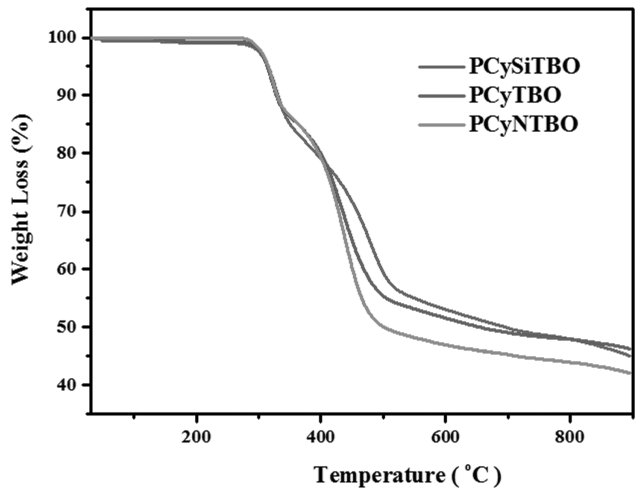

FIGURE 1 TGA thermograms of the polymers **PCyTBO**, **PCySiTBO**, and **PCyNTBO**, recorded at a heating rate of 20°C min^{-1} under a N_2 atmosphere.

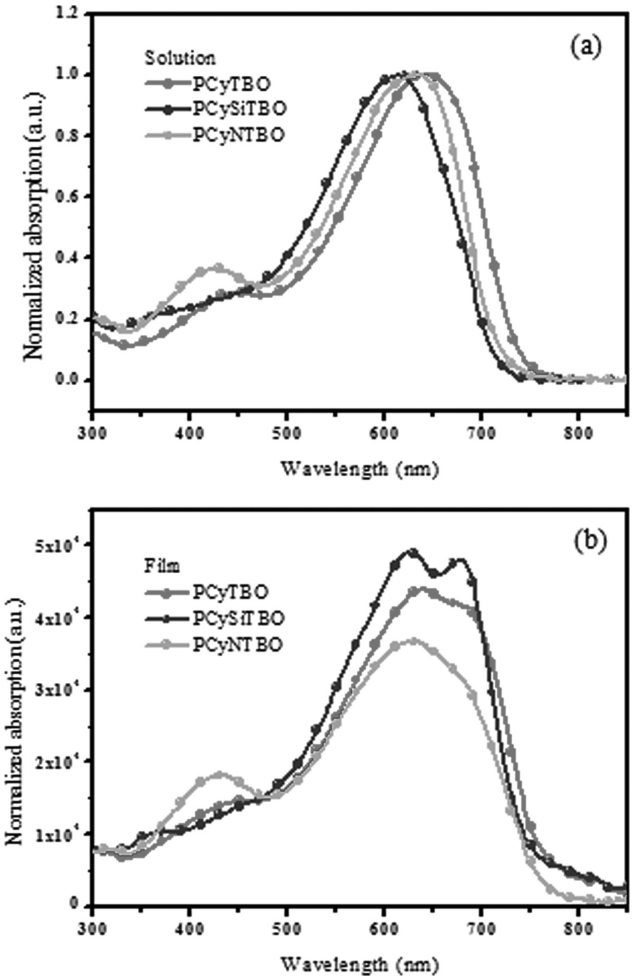

FIGURE 2 UV–Vis absorption spectra of the polymers **PCyTBO**, **PCySiTBO**, and **PCyNTBO** as (a) dilute solutions in DCB (1×10^{-5} M) and (b) solid films.

TABLE 2 Optical Properties of **PCyTBO**, **PCySiTBO**, and **PCyNTBO**

	$\lambda_{max,abs}$ (nm)		λ_{onset} (nm)	
	Solution	Film	Film	E_g^{opt} (eV)
PCyTBO	640	645	777	1.59
PCySiTBO	611	623, 678	756	1.64
PCyNTBO	631	632	777	1.59

potentials, we estimated the HOMO and LUMO energy levels according to the energy level of the ferrocene reference (4.8 eV below vacuum level).[41,42] The HOMO energy levels of **PCyTBO**, **PCySiTBO**, and **PCyNTBO** were −4.98, −5.02, and −4.89 eV, respectively, implying that they varied with respect to the modulated ICT strengths resulting from the presence of electron donors with various electron-donating abilities,[43–45] or more precisely, the HOMO energy levels of these polymers become higher as the electron-donating ability of C-, Si-, or N-bridged dithiophene units increases. The LUMO energy levels of **PCyTBO**, **PCySiTBO**, and **PCyNTBO** were all located within a reasonable range (from −2.8 to −3.0 eV, Fig. 4) and were significantly greater than that of $PC_{61}BM$ (ca. 4.1 eV); thus, we expected efficient charge transfer/dissociation to occur in their corresponding devices.[46,47] In addition, the electrochemical band gaps (E_g^{ec}) of **PCyTBO**, **PCySiTBO**, and **PCyNTBO**, estimated from the difference between the onset potentials for oxidation and reduction, were in the range of 1.94–2.08 eV; that is, they were slightly larger than the corresponding optical band gaps. The discrepancy between the electrochemical and the optical band gaps presumably resulted from the exciton binding energies of the polymers and/or the interfacial barriers for charge injection.[48]

The band gap and HOMO/LUMO energy levels of a typical polymer originate from molecular orbital hybridization of the donor and acceptor energy levels in the D/A-type polymers. Therefore, electron-donating groups will decrease the value of E_g by increasing the HOMO energy level in the polymer. In our case, we expected the cyclopentadithiophene donor unit in **PCyTBO** and the dithienosilole donor unit in **PCySiTBO** to have similar electron-donating abilities, owing to their similar experimental band gaps and energy levels (Table 3). For the **PCyNTBO** polymer, however, the electron-donating ability of the N atom is much stronger than those of both the C and the Si atoms; therefore, we found a lower band gap and higher HOMO energy level for this polymer.

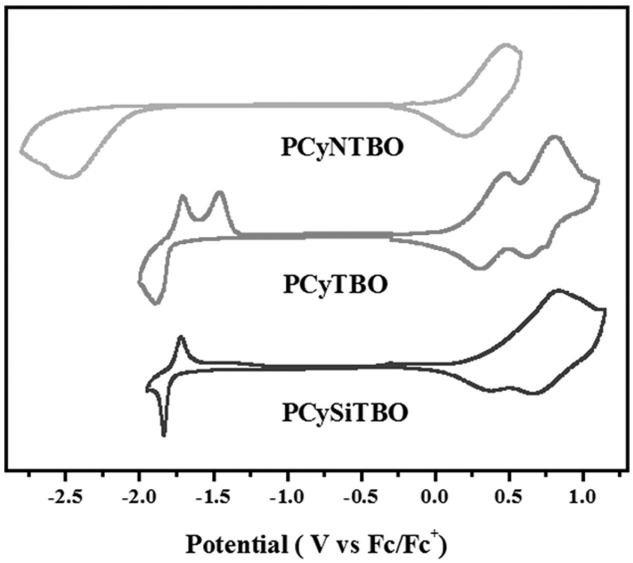

FIGURE 3 Cyclic voltammograms of solid films of the polymers **PCyTBO**, **PCySiTBO**, and **PCyNTBO**.

Computational Study

We performed computational analyses of **PCyTBO**, **PCySiTBO**, and **PCyNTBO** to obtain insight into the observed differences between their optical and electrochemical properties. To simplify the calculations, we subjected only one repeating unit of each polymer to the calculation, with the alkyl chains replaced by CH_3 groups. Figure 5 shows the simulated electron density distributions; Table 3 lists the calculated HOMO and LUMO energy levels. The calculations for the HOMO revealed extended delocalization along the entire conjugated backbone, affected by both the donor and the acceptor units. Similarly, the calculated density of states for the LUMO also displayed an extended distribution across the entire conjugated backbone, but with more of an effect on the acceptor units. In addition, the effects of the bridging atom in the dithiophene unit were quite discrete for both the HOMO and the LUMO electron density distributions. The densities of the respective HOMO wave functions were distributed across the fused heteroaromatic backbones, with less density on the electron-accepting substituents. For the LUMO, electron densities were localized to a greater degree on the respective electron acceptor units and at the center of the fused aromatic backbone. Upon changing the "CyN" unit to the weaker-donor "Cy" and "CySi" units, the calculated HOMO energy levels of **PCyTBO** and **PCySiTBO** were lower than that of **PCyNTBO**. The LUMO energy levels of the three

TABLE 3 Electrochemical Properties of **PCyTBO**, **PCySiTBO**, and **PCyNTBO**

	E_{onset}^{ox} (V)	E_{onset}^{red} (V)	HOMO[a] (eV)	LUMO[a] (eV)	E_g^{ec} (eV)	HOMO[b] (eV)	LUMO[b] (eV)
PCyTBO	0.18	−1.76	−4.98	−3.04	1.94	−4.70	−2.45
PCySiTBO	0.22	−1.76	−5.02	−3.04	1.98	−4.75	−2.45
PCyNTBO	0.09	−1.99	−4.89	−2.81	2.08	−4.64	−2.40

[a] HOMO and LUMO energy levels estimated from the oxidation and reduction peaks, respectively, of the cyclic voltammograms.

[b] HOMO and LUMO energy levels calculated using DFT.

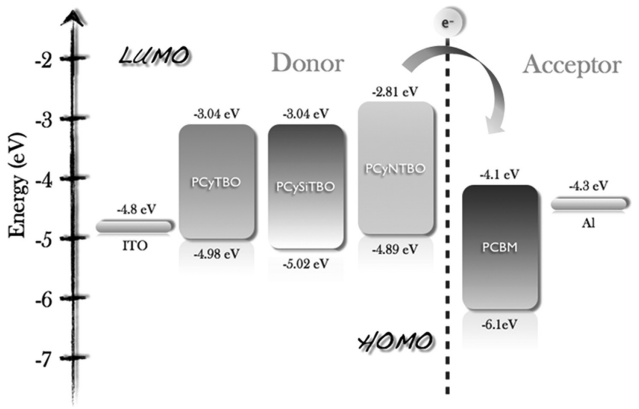

FIGURE 4 Energy level diagram for **PCyTBO**, **PCySiTBO**, and **PCyNTBO**.

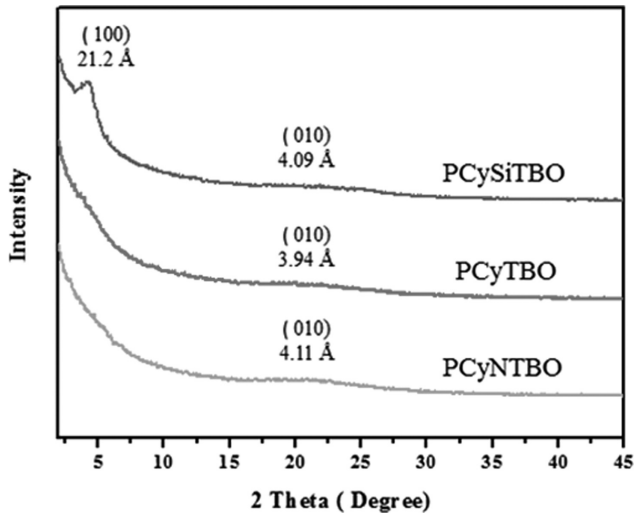

FIGURE 6 X-ray diffraction patterns of pristine **PCyTBO**, **PCySiTBO**, and **PCyNTBO** films.

polymers were, however, identical, because they shared the same acceptor unit, TBO. The results from the calculations follow the same trend as those observed from the experimental values.

X-Ray Diffraction Patterns

We recorded grazing-incidence X-ray diffraction patterns to confirm the crystallinity of the thin films of these polymers (Fig. 6). The (100) peak for **PCySiTBO** appeared at 4.16°, indicating a ordered structure with a *d*-spacing of 21.2 Å, ascribable to the interchain separation of the alkyl side chains; we assign a broad feature at 21.7°, corresponding to a short distance of 4.1 Å, to facial π–π stacking of the polymeric backbones. The grazing-incidence X-ray diffraction patterns of **PCyTBO** and **PCyNTBO** featured only broad reflections at 22.5 and 21.6°, respectively, to their (010) crystal plane, corresponding to distances of 3.9 and 4.1 Å, respectively, and suggesting facial π–π stacking of the polymeric chains. The crystallinity of these polymers appeared to be favorable for charge transport within PSCs.

Hole Mobility

Figure 7 shows the hole mobilities of devices incorporating the pristine polymers and the polymer/PCBM blends at a blend ratio of 1:1 (w/w). The hole mobilities of the pristine **PCyTBO**, **PCySiTBO**, and **PCyNTBO** were 3.2×10^{-4}, 9.8×10^{-4}, and 1.8×10^{-4} cm^2 V^{-1} s^{-1}, respectively, whereas those of the **PCyBO**, **PCySiTBO**, and **PCyNTBO** blends with $PC_{61}BM$ were 9.1×10^{-5}, 1.6×10^{-4}, and 3.3×10^{-5} cm^2 V^{-1} s^{-1}, respectively. Thus, the hole mobility of **PCySiTBO** was greater than that of **PCyTBO** or **PCyNTBO**, presumably

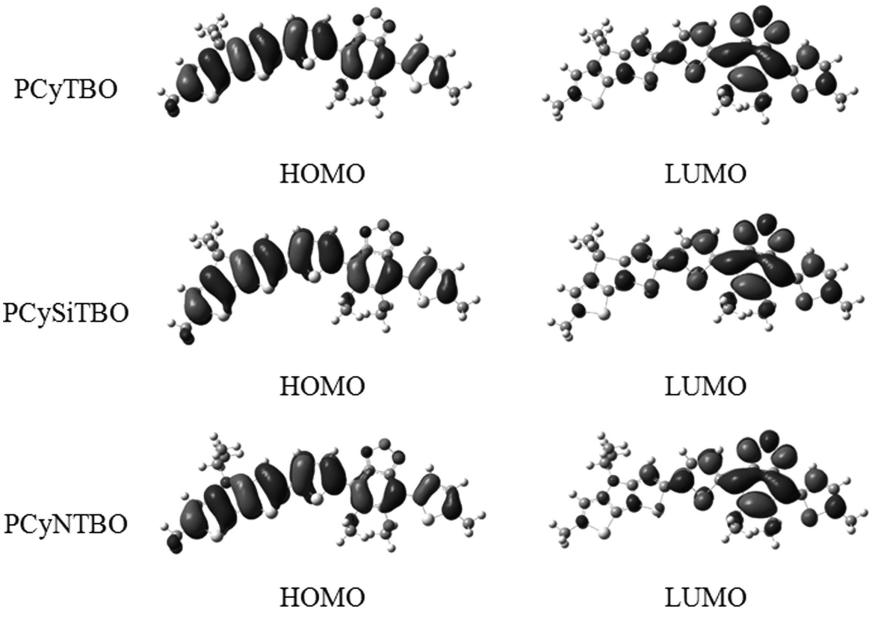

FIGURE 5 Simulated HOMO and LUMO electron density distributions of **PCyTBO**, **PCySiTBO**, and **PCyNTBO**, determined through density functional theory (DFT) calculations.

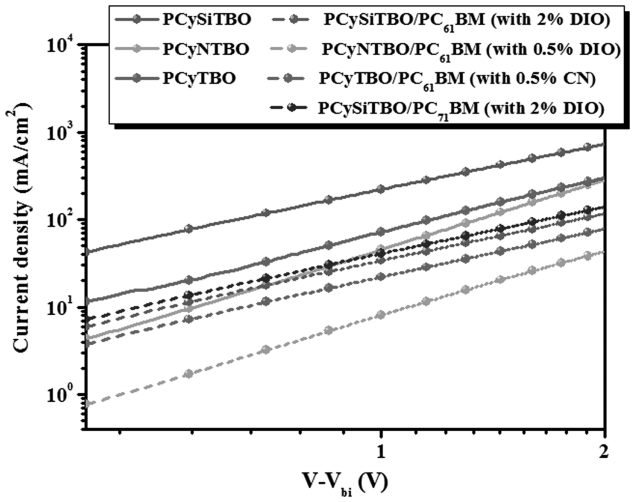

FIGURE 7 Dark *J–V* curves for the hole-dominated carrier devices incorporating the pristine polymers and the blend films prepared at a blend ratio of 1:1 (w/w).

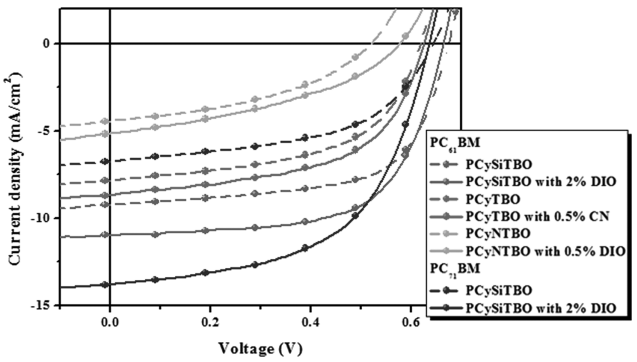

FIGURE 8 *J–V* characteristics of PSCs incorporating polymer:$PC_{61}BM$ and polymer:$PC_{71}BM$ blends (blend ratio, 1:1 (w/w)) in the presence and absence of CN or DIO.

because of the greater crystallinity and the longer C—Si bond (~0.3Å) in **PCySiTBO** that allows for better interchain polymer packing for improving its hole mobility.[38]

Photovoltaic Properties

Next, we investigated the photovoltaic properties of the polymers in BHJ solar cells having the sandwich structure ITO/PEDOT:PSS/polymer:PCBM (1:1, w/w)/Ca/Al, with the photoactive layers having been spin-coated from DCB solutions of the polymer and PCBM. The optimized weight ratio for the polymer and PCBM was 1:1. In this case, we added a small amount of 1,8-diiodooctane (DIO; 0.5–3% by volume, relative to DCB) and 1-chloronaphthalene (CN; 0.5–3% by volume, relative to DCB) to optimize the miscibility of the blends. Figure 8 shows the *J–V* curves of these PSCs; more than 10 devices were fabricated and their average PCEs are summarized in Table 4. The devices prepared from the polymer:$PC_{61}BM$ blends of **PCyTBO**, **PCySiTBO**, and **PCyNTBO** exhibited open-circuit voltages (V_{oc}) of 0.62, 0.68, and 0.52 V, respectively; each value is related to the difference between the HOMO energy level of the polymer and the LUMO energy level of $PC_{61}BM$.[49] We suspect that the **PCyNTBO** blend provided the lowest value of V_{oc} because of its relatively higher-lying HOMO energy level. The short-circuit current densities (J_{sc}) of the devices incorporating **PCyTBO**, **PCySiTBO**, and **PCyNTBO** were 7.9, 9.2, and 4.5 mA cm^{-2}, respectively. Furthermore, when we incorporated DIO and CN into the 1:1 (w/w) polymer:$PC_{61}BM$ blends, the devices based on **PCyTBO**, **PCySiTBO**, and **PCyNTBO** exhibited slightly increased values of J_{sc} of 8.6, 10.8, and 5.1 mA cm^{-2}, respectively, resulting in increased PCEs. Figure 9 shows the EQE curves of the devices incorporating the polymer:$PC_{61}BM$ blends at weight ratios of 1:1, with 0.5 vol % CN as the additive for **PCyTBO**, 2 vol % DIO as the additive for **PCySiTBO**, and 0.5 vol % DIO as the additive for **PCyNTBO**. The theoretical short-circuit current densities obtained from integrating the EQE curves of the **PCyTBO**, **PCySiTBO**, and **PCyNTBO** blends were 8.2, 10.2, and 4.9 mA cm^{-2}—values that agree reasonably with the measured (AM 1.5 G) values of J_{sc} of 8.6, 10.8, and 5.1 mA cm^{-2}, respectively, with discrepancies of <6%. We attribute this higher value of J_{sc} of **PCySiTBO** to its higher absorption coefficient [Fig. 2(b)]; consistently, the EQE curve also featured higher EQE responses at 350–700 nm. Thus, more of the available

TABLE 4 Photovoltaic Properties of PSCs Incorporating BO-Based Polymers

Polymer/$PC_{61}BM$ (1:1) (w/w)	V_{oc} (V)	J_{sc} (mA cm^{-2})	FF (%)	PCE_{max} ($PCE_{average}$)[a] (%)	Mobility (cm^2 V^{-1} s^{-1})	Thickness (nm)
PCyTBO	0.62	7.9	54	2.6 (2.45)		88
PCyTBO[b]	0.63	8.6	56	3.0 (2.93)	9.1×10^{-5}	87
PCySiTBO	0.68	9.2	64	4.0 (3.88)		101
PCySiTBO[c]	0.66	10.8	66	4.7 (4.52)	1.6×10^{-4}	97
PCyNTBO	0.52	4.5	42	1.0 (0.96)		90
PCyNTBO[d]	0.58	5.1	42	1.2 (1.15)	3.3×10^{-5}	95
Polymer/$PC_{71}BM$ (1:1) (w/w)						
PCySiTBO	0.64	6.7	53	2.3 (2.21)		99
PCySiTBO[c]	0.64	13.8	57	5.0 (4.91)	2×10^{-4}	103

[a] More than 10 devices were fabricated.
[b] Processed with 0.5 vol % CN.
[c] Processed with 2 vol % DIO.
[d] Processed with 0.5 vol % DIO.

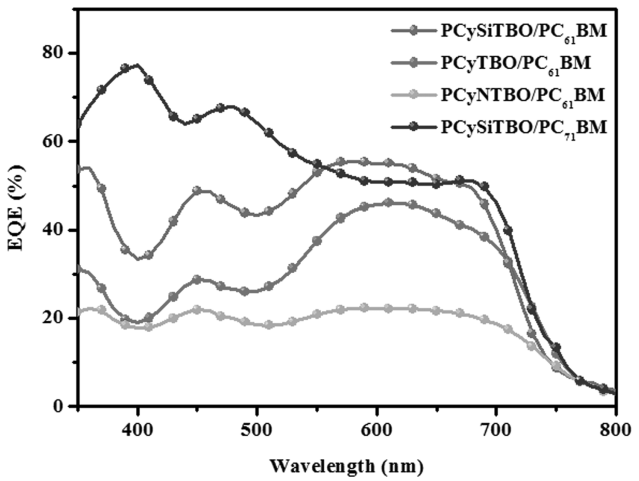

FIGURE 9 EQE curves of PSCs incorporating polymer:$PC_{61}BM$ and polymer:$PC_{71}BM$ blends (blend ratio, 1:1 (w/w)), with 0.5% CN as the additive for **PCyTBO**, 2% DIO as the additive for **PCySiTBO**, and 0.5% DIO as the additive for **PCyNTBO**.

photons from the solar radiation were absorbed by **PCySiTBO**, leading to higher photocurrents for its devices. Moreover, we also fabricated a solar cell device incorporating **PCySiTBO** and $PC_{71}BM$ as the active layer. In Figure 9, we observe higher quantum efficiency at wavelengths below 550 nm for the **PCySiTBO**/$PC_{71}BM$ device than for the **PCySiTBO**/$PC_{61}BM$, which is presumably caused by the absorption of $PC_{71}BM$ in the shorter-wavelength range. The short circuit current density of the device incorporating 1:1 (w/w) **PCySiTBO**/$PC_{71}BM$ blend as the active layer device increased dramatically when adding 2% DIO into the processing solvent as compared to the **PCySiTBO**/$PC_{71}BM$ device processed without the additive DIO, 13.8 vs. 6.7 mA cm^{-2}. As a result, the device based on **PCySiTBO**/$PC_{71}BM$ (1:1) active layer that was processed with DIO additive exhibited the highest values of PCE, 5.0%.

The higher FF of the device incorporating **PCySiTBO**:$PC_{61}BM$ (1:1, w/w) as the active layer with 2 vol % DIO as the additive was likely owing to the higher hole mobility of the active layer (Fig. 7); the hole mobilities of **PCySiTBO** and **PCySiTBO**:$PC_{61}BM$ (1:1, w/w) were larger than those of **PCyTBO**, **PCyNTBO**, **PCyTBO**:$PC_{61}BM$, and **PCyNTBO**:$PC_{61}BM$. Therefore, we attribute the enhanced FF to the increased hole mobility in the active layer—most likely caused by the crystallinity in the **PCySiTBO** active layer being greater than those in the **PCyTBO** and **PCyNTBO** active layers.[29]

Moreover, when exploring the decisive factors affecting the efficiencies of PSCs, we must consider not only the absorption and energy levels of polymers but also the surface morphologies of the polymer blends. Figure 10 shows the surface morphologies of our systems, determined using AFM. Samples of the polymer:PCBM blends were prepared using procedures identical to those used to fabricate the active layers of the devices. In each case, we observed no obviously aggregate morphology (R_{ms} = 0.5–1.3 nm) of the polymer blend [Fig. 11(a–d)]. Furthermore, when we incorporated the additive into the polymer/PCBM blend, their morphology presented a moderately homogeneous morphology (R_{ms} = 1–1.4 nm). The incorporation of CN (0.5 vol %) into the 1:1

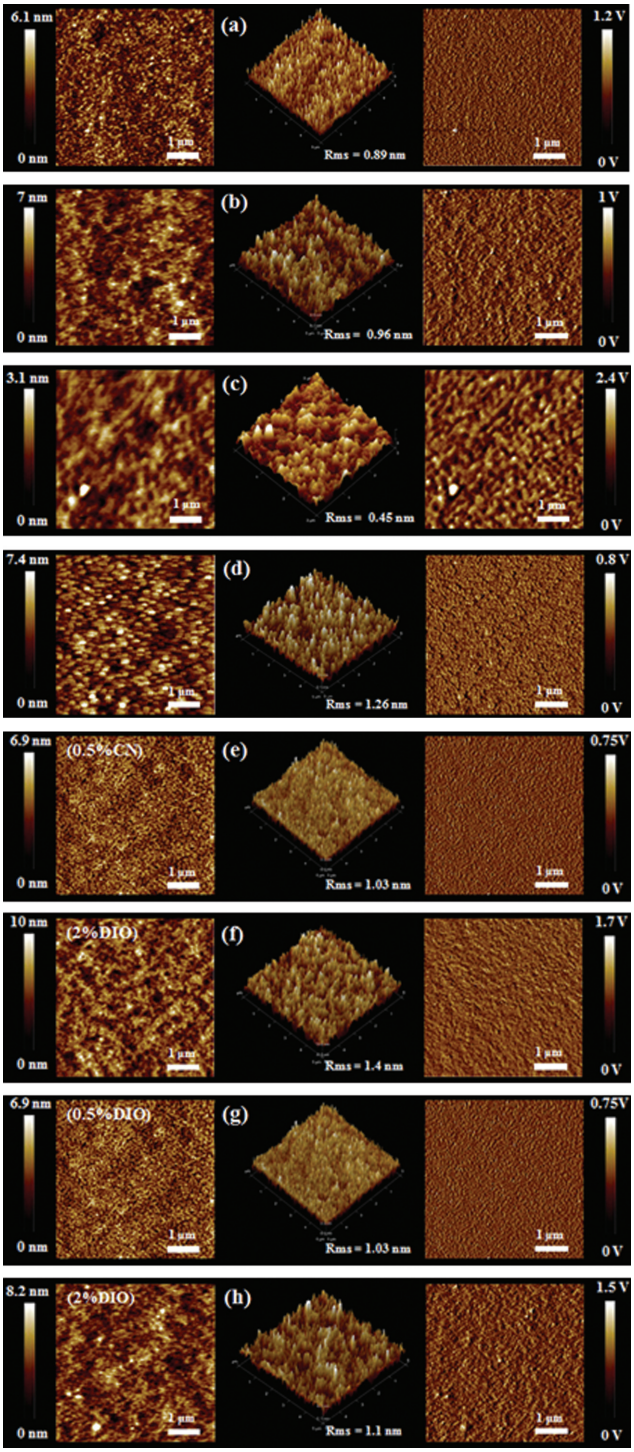

FIGURE 10 Topographic AFM images of polymer:$PC_{61}BM$ (1:1, w/w) blends incorporating (a) **PCyTBO**, (b) **PCySiTBO**, (c) **PCyNTBO**, (e) **PCyTBO** and 0.5 vol % CN, (f) **PCySiTBO** and 2 vol % DIO, and (g) **PCyNTBO** and 0.5 vol % DIO, and polymer:$PC_{71}BM$ (1:1, w/w) blends incorporating (d) **PCySiTBO**, (h) **PCySiTBO** with 2 vol % DIO.

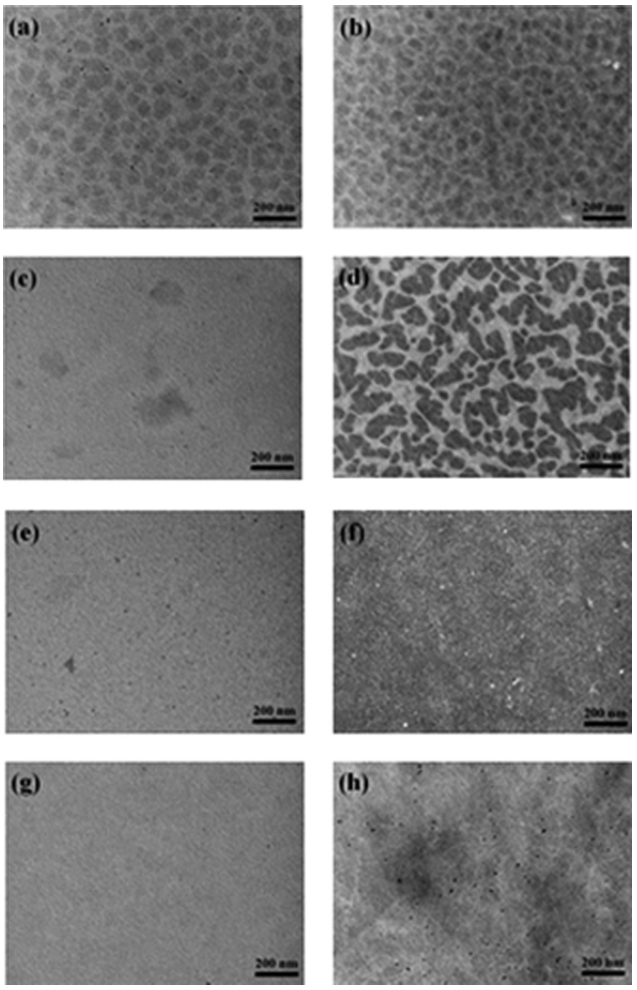

FIGURE 11 TEM images of polymer:$PC_{61}BM$ (1:1, w/w) blends incorporating (a) **PCyTBO**, (b) **PCySiTBO**, (c) **PCyNTBO**, (e) **PCyTBO** and 0.5 vol % CN, (f) **PCySiTBO** and 2 vol % DIO, and (g) **PCyNTBO** and 0.5 vol % DIO, and polymer:$PC_{71}BM$ (1:1, w/w) blends incorporating (d) **PCySiTBO**, (h) **PCySiTBO** with 2 vol % DIO.

(w/w) **PCyTBO**:$PC_{61}BM$ blend, the device exhibited slightly increased values of J_{sc} and FF of 8.6 mA cm^{-2} and 0.56, respectively, resulting in an increased PCE of 3.0%. The incorporation of DIO (2 vol %) into the 1:1 (w/w) **PCySiTBO**:$PC_{61}BM$ and **PCySiTBO**:$PC_{71}BM$ blend increased the value of J_{sc} to 10.8 and 13.8 mA cm^{-2}, increased the FF slightly to 0.66 and 0.57, therefore enhanced the PCE to 4.7 and 5.0%, presumably because more-intimate mixing of **PCyTBO** and **PCySiTBO** [Fig. 11(e–g)]. The incorporation of DIO (0.5 vol %) into the 1:1 (w/w) **PCyNTBO**:$PC_{61}BM$ blend had almost no impact on the values of J_{sc} and efficiency (remaining at 1.2%). Figure 11 shows TEM images of the polymer/PCBM blend films. As the electron scattering density of PCBM was higher than that of the conjugated polymer, the polymer domains appear as bright regions; the dark regions are attributed to PCBM domains. Figure 11(a,b,d) shows the island-shaped features of the aggregated $PC_{61}BM$ and $PC_{71}BM$ domains (dark areas) in the blend films with **PCyTBO**/$PC_{61}BM$, **PCySiTBO**/$PC_{61}BM$, and **PCySiTBO**/$PC_{71}BM$ (weight ratios, 1:1), respectively, that we processed without additives. In contrast, Figure 11(e,f,h) shows the homogeneous morphologies of the **PCyTBO**/$PC_{61}BM$ **PCySiTBO**/$PC_{61}BM$ and **PCySiTBO**/$PC_{71}BM$ blend films (weight ratios, 1:1) that we processed with CN (0.5 vol %) and DOI (2 vol %) as additives, indicating that the incorporation of the additives optimized the miscibility of the polymer chains with PCBM. Through optimization of the blend morphology, such high values of J_{sc}, FF, and PCE were also possible for the polymer:PCBM blends at a weight ratio of 1:1. Incorporation of DIO (0.5 vol %) into the 1:1 (w/w) **PCyNTBO**:$PC_{61}BM$ blend film resulted in the same morphology and miscibility as that of the nonadditive films, while maintaining the efficiency at 1.2%.

CONCLUSIONS

We have used Stille coupling polymerization to prepare a series of new crystalline, conjugated polymers—**PCyTBO, PCySiTBO**, and **PCyNTBO**—featuring alternating C-, Si-, and N-bridged dithiophene-based building blocks and BO units in their backbones. These polymers exhibit broad absorption and good thermal stability, and **PCySiTBO** possess good crystallinity, making them promising materials for solar cell applications. A device incorporating **PCySiTBO** and $PC_{71}BM$ (blend weight ratio, 1:1), with DIO (2 vol %) as an additive, exhibited a value of V_{oc} of 0.64 V, a value of J_{sc} of 13.8 mA cm^{-2}, a FF of 0.57, and a PCE of 5.0%.

ACKNOWLEDGMENTS

The authors thank the National Science Council, Taiwan, for financial support (NSC 98-2120-M-009-006).

REFERENCES AND NOTES

1 Zhang, S.; Guo, Y.; Fan, H.; Liu, Y.; Chen, H. Y.; Yang, G.; Zhan, X.; Liu, Y.; Li Y.; Yang, Y. *J. Polym. Sci A Polym. Chem.* **2009,** *47*, 5498–5508.

2 Wienk, M. M.; Koon, J. M.; Verhees, W. J. H.; Knol, J.; Hummelen, J. C.; Vanhal, P. A.; Janssen, R. A. *J. Angew. Chem. Int. Ed.* **2003,** *42*, 3371.

3 Dennler, G.; Scharber, M. C.; Brabec, C. *J. Adv. Mater.* **2009,** *21*, 1323.

4 Shaheen, S. E., Brabec, C. J., Sariciftci, N. S., Padinger, F., Fromherz, T.; Hummelen, J. C. *Appl. Phys. Lett.* **2001,** *78*, 841–843.

5 Ma, W.; Yang, C.; Gong, X.; Lee, K.; Heeger, A. *J. Adv. Funct. Mater.* **2005,** *15*, 1617.

6 Kim, Y.; Cook, S.; Tuladhar, S. M.; Choulis, S. A.; Nelson, J.; Durrant, J. R.; Bradley, D. D. C.; Giles, M.; McCulloch, I.; Ha, C. S.; Ree, M. *Nat. Mater.* **2006,** *5*, 197.

7 Kim, J. Y.; Lee, K.; Coates, N. E.; Moses, D.; Nguyen, T. Q.; Dante, M.; Heeger, A. J. *Science* **2007,** *317*, 222.

8 Bundgaard, E.; Krebs, F. C. *Sol. Energy Mater. Sol. Cells* **2007,** *91*, 954.

9 Bijleveld, J. C.; Gevaert, V. S.; Nuzzo, D. D.; Turbiez, M.; Mathijssen, S. G. J.; Leeuw, D. M.; Wienk, M. M.; Janssen, R. A. *J. Adv. Mater.* **2010,** *22*, E242.

10 Zhang, Y.; Hau, S. K.; Yip, H. L.; Sun, Y.; Acton, O.; Jen, A. K. Y. *Chem. Mater.* **2010,** *22*, 2696.

11 Zhang, Y.; Zou, J.; Yip, H. L.; Chen, K. S.; Davies, J. A.; Sun, Y.; Jen, A. K. J. *Macromolecules* **2011,** *44*, 4752.

12 Jiang, J. M.; Yang, P. A.; Chen H. C.; Wei, K. H. *Chem. Commun.* **2011,** *47*, 8877.

13 Zhang, M. J.; Guo, X.; Li, Y. F. *Macromolecules* **2011,** *44*, 8798.

14 Song, J. S.; Du, C.; Li, C. H.; Bo, Z. H. *J. Polym. Sci. Part A: Polym. Chem.* **2011,** *49*, 4267.

15 Bijleveld, J. C.; Verstrijden, R. A. M.; Wienk, M. M.; Janssen, R. A. J. *J. Mater. Chem.* **2011,** *21*, 9224.

16 Wang, X. C.; Luo, H.; Sun, Y. P.; Zhang, M. J.; Li, X. Y.; Yu, G.; Liu, Y. Q.; Li, Y. F.; Wang, H. Q. *J. Polym. Sci. Part A: Polym. Chem.* **2012,** *50*, 371.

17 Sun, Y.; Chien, S. C.; Yip, H. L.; Zhang, Y.; Chen, K. S.; Zeigler, D. F.; Chen, F. C.; Lin, B.; Jen, A. K. Y. *J. Mater. Chem.* **2011,** *21*, 13247.

18 Laure, B.; Christos, L. C.; Nicolas, L.; Olivier, B.; Sadiara, F.; Patrick, L.; Thomas, M. *J. Polym. Sci. Part A: Polym. Chem.* **2012,** *50*, 1861.

19 Wang, X. C.; Sun, Y. P.; Chen, S.; Guo, X.; Zhang, M. J.; Li, X. Y.; Li Y. F.; Wang, H. Q. *Macromolecules* **2012,** *45*, 1208.

20 Yuan, M. C.; Su, M. H.; Chiu, M. Y.; Wei, K. H. *J. Polym. Sci. Part A: Polym. Chem.* **2009,** *48*, 1298.

21 Hsu, S. L.; Chen, C. M.; Wei, K. H. *J. Polym. Sci. Part A: Polym. Chem.* **2010,** *48*, 5126.

22 Huang, F.; Chen, K. S.; Yip, H. L.; Hau, S. K.; Acton, O.; Zhang, Y.; Luo, J.; Jen, A. K. Y. *J. Am. Chem. Soc.* **2009,** *131*, 13886.

23 Zhang, Z. G.; Liu, Y. L.; Yang, Y.; Hou, K.; Peng, B.; Zhau, G.; Zhang, M. J.; Guo, X.; Kang, E. T.; Li, Y. F. *Macromolecules* **2010,** *43*, 9376.

24 Zhang, Z. G.; Zhang, S.; Ming, J.; Chui, C. H.; Zhang, J.; Zhang, M. J.; Li, Y. F. *Macromolecules,* **2012,** *45*, 113.

25 Chen, H. Y.; Hou, J. H.; Zhang, S. Q.; Liang, Y. Y.; Yang, G. W.; Yang, Y.; Yu, L. P.; Wu, Y.; Li, G. *Nat. Photonics* **2009,** *3*, 649.

26 Son, H. J.; Wang, W.; Xu, T.; Liang, Y. Y.; Wu, Y.; Li, G.; Yu, L. P. *J. Am. Chem. Soc.* **2011,** *133*, 1885.

27 Chu, T. Y.; Lu, J.; Beaupre, S.; Zhang, Y.; Pouliot, J. R.; Wakim, S.; Zhou, J.; Leclerc, M.; Li, Z.; Ding, J.; Tao, Y. *J. Am. Chem. Soc.* **2011,** *133*, 4250.

28 Price, S. C.; Stuart, A. C.; Yang, L.; Zhou, H.; You, W. *J. Am. Chem. Soc.* **2011,** *133*, 4625.

29 Su, M. S.; Kuo, C. Y.; Yuan, M. C.; Jeng, U. S.; Su C. J.; Wei, K. H. *Adv. Mater.* **2011,** *23*, 3315.

30 Zhu, Z.; Waller, D.; Gaudiana, R.; Morana, M.; Muhlbacher, D.; Scharber, M.; Brabec, C. J. *Macromolecules* **2007,** *40*, 1981.

31 Lee, K. J.; Ma, L. W.; Brabec, C. J.; Yuen, J.; J. Moon, S.; Kim, J. Y.; Lee, K.; Bazan, G. C.; and Heeger, A. J. *J. Am. Chem. Soc.* **2008,** *130*, 3619.

32 Bijleveld, J. C.; Shahid, M.; Gilot, J.; Wienk, M. M.; Janssen, R. A. *J. Adv. Funct. Mater.* **2009,** *19*, 3262.

33 Zhan, X. W.; Risko, C.; Amy, F.; Chan, C.; Zhao, W.; Barlow, S.; Kahn, A.; Bredas, J. L.; Marder, S. R. *J. Am. Chem. Soc.* **2005,** *127*, 9021.

34 Lu, G.; Usta, H.; Risko, C.; Wang, L.; Facchetti, A.; Ratner, M. A.; Marks, T. J. *J. Am. Chem. Soc.* **2008,** *130*, 7670.

35 Hou, L. J.; Yu, H.; Hou, J. H.; Chen, T. L.; Yang, Y. *Chem. Commun.* **2009,** *37*, 5570.

36 Zhou, E. J.; Nakamura, M.; Nishizawa, T.; Zhang, Y.; Wei, Q. S.; Tajima, K.; Yang, C. H.; Hashimoto, K. *Macromolecules,* **2008,** *41*, 8302.

37 Zhou, E. J.; Wei, Q. S.; Yamakawa, S.; Zhang, Y.; Tajima, K.; Yang, C. H.; Hashimoto, K. *Macromolecules,* **2010,** *43*, 821.

38 Jiang, J. M.; Yang, P. A.; Hsieh T. H.; Wei, K. H. *Macromolecules,* **2011,** *44*, 9155.

39 Zhang, Y.; Zou, J.; Yip, H. L.; Sun, Y.; Davies, J. A.; Chen, K. S.; Acton, O.; Jen, A. K. Y. *J. Mater. Chem.* **2011,** *21*, 3895.

40 Melzer, C.; Koop, E. J.; Mihailetchi, V. D.; Blom, P. W. *Adv. Funct. Mater.* **2004,** *14*, 865.

41 Pommerehne, J.; Vestweber, H.; Guss, W.; Mahrt, R. F.; Bassler, H.; Porsch, M.; Daub, J. *Adv. Mater.* **1995,** *7*, 551.

42 Liang, Y.; Feng, D.; Wu, Y.; Tsai, S. T.; Li, G.; Ray, C.; Yu, L. P. *J. Am. Chem. Soc.* **2009,** *131*, 7792.

43 Zou, Y.; Gendron, D.; Neagu, R.; Leclerc, M. *Macromolecules,* **2009,** *42*, 6361.

44 Huo, L.; Hou, J.; Chen, H. Y.; Zhang, S.; Jiang, Y.; Chen, T. L.; Yang, Y. *Macromolecules* **2009,** *42*, 6564.

45 Zhu, Y.; Champion, R. D.; Jenekhe, S. A. *Macromolecules* **2006,** *39*, 8712.

46 Thompson, B. C.; Frechet, J. M. *Angew. Chem. Int. Ed.* **2008,** *47*, 58.

47 Scharber, M. C.; Muhlbacher, D.; Koppe, M.; Denk, P.; Waldauf, C.; Heeger, A. J.; Brabec, C. *J. Adv. Mater.* **2006,** *18*, 789.

48 Wu, P. T.; Kim, F. S.; Champion, R. D.; Jenekhe, S. A. *Macromolecules* **2008,** *41*, 7021.

49 Brabec, C. J.; Cravino, A.; Meissner, D.; Sariciftci, N. S.; Fromherz, T.; Rispens, M. T.; Sanchez, L.; Hummelen, J. C. *Adv. Funct. Mater.* **2001,** *11*, 374.